Available online at www.sciencedirect.com
SCIENCE DIRECT®
Journal of Solid State Chemistry 178 (2005) 2144–2151
JOURNAL OF SOLID STATE CHEMISTRY
www.elsevier.com/locate/jssc

Crystal structure, phase transition and anisotropic thermal expansion of barium zirconium diorthophosphate, $BaZr(PO_4)_2$

Koichiro Fukuda*, Akira Moriyama, Tomoyuki Iwata

Department of Environmental and Materials Engineering, Nagoya Institute of Technology, Nagoya 466-8555, Japan

Received 22 February 2005; received in revised form 12 April 2005; accepted 19 April 2005

Abstract

The crystal structure of $BaZr(PO_4)_2$ at 298 K was determined from conventional X-ray powder diffraction data using direct methods, and it was further refined by the Rietveld method. The structure was monoclinic (space group $C2/m$, $Z = 2$) with $a = 0.85629(3)$ nm, $b = 0.53082(2)$ nm, $c = 0.78956(2)$ nm, $\beta = 93.086(1)^\circ$ and $V = 0.35836(2)$ nm^3. Final reliability indices were $R_{wp} = 8.21\%$, $R_p = 5.64\%$ and $R_B = 2.92\%$. The atom arrangement is similar to that of yavapaiite ($KFe(SO_4)_2$), however, these crystal structures differ distinctly in the coordination numbers of barium and potassium atoms; the former is tenfold coordinated, whereas the latter is sixfold coordinated. The powder specimens were also examined by high-temperature XRD and DTA to reveal the occurrence of a phase transition from monoclinic to orthorhombic at 732 K during heating. Upon cooling the reverse transition occurred at 710 K. The monoclinic crystal expanded almost one-dimensionally along [503] during the heating process. The orthorhombic phase also showed a tendency to expand one-dimensionally along the c-axis above 732 K.

Keywords: Barium zirconium diorthophosphate; Phase transition; High-temperature XRD; Rietveld method; Thermal expansion

1. Introduction

Double phosphates such as $MZr(PO_4)_2$ with $M = Ca$, Sr and Ba are promising materials as catalysts, ion exchangers and ion conductors. The compound $SrZr(PO_4)_2$ undergoes two phase transitions from triclinic to monoclinic, then to hexagonal (or trigonal) during heating [1]. The monoclinic phase is most probably isostructural with yavapaiite ($KFe(SO_4)_2$, space group $C2/m$) [2] as judged by the similarity in powder XRD pattern. The triclinic and hexagonal phases can be therefore described as, respectively, the lower- and higher-temperature polymorphs of the yavapaiite-type structure. The structure of $CaZr(PO_4)_2$ is distinct from that of yavapaiite. This compound is orthorhombic with space group $P2_12_12_1$ and free from polymorphic phase transitions [3]. With $BaZr(PO_4)_2$, neither the crystal structure nor polymorphic sequence has been reported so far.

When a crystal is uniformly heated, it homogeneously deforms and as a result expands uniformly. Because of anisotropy of the crystals except for the cubic system, the thermal deformation depends on direction. If the initial crystal has a spherical shape, the resulting crystal after heating will be ellipsoidal. There are three directions perpendicular to each other along the principal axes of the ellipsoid [4,5]. With crystals belonging to the orthorhombic system, the principal axes are exactly parallel to the crystallographic axes. However, with crystals belonging to the monoclinic system, one of the principal axes of deformation is parallel to the diad axis (b-axis for second setting), and the two others do not necessarily coincide with the crystallographic axes. The magnitudes and directions of the principal distortions are readily determined from calculations based on matrix algebra analysis of the temperature dependence of cell dimensions.

*Corresponding author. Fax: +81 52 735 5289.
E-mail address: fukuda.koichiro@nitech.ac.jp (K. Fukuda).

0022-4596/$ - see front matter © 2005 Elsevier Inc. All rights reserved.
doi:10.1016/j.jssc.2005.04.022

In the present study, we have determined the crystal structure of $BaZr(PO_4)_2$ from powder XRD data using direct methods. The powder specimens were further examined at high temperatures to demonstrate the thermal expansion anisotropy and occurrence of a phase transition.

2. Experimental

2.1. Synthesis

The present specimen of barium zirconium diorthophosphate $BaZr(PO_4)_2$ was prepared from stoichiometric amounts of reagent-grade chemicals $BaCO_3$, ZrO_2 and $NH_4H_2PO_4$. A mixture of the former two chemicals was first heated at 1773 K for 1 h in order to synthesize the crystals of $BaZrO_3$. Then, the product was mixed with the latter. The mixture was pressed into pellets (12 mm diameter and 3 mm thick), heated at 1573 K for 100 h, followed by quenching in air.

2.2. Crystal structure determination

X-ray powder diffraction intensities for structural determination were collected at 298 K on a PANalytical X'Pert diffractometer in Bragg–Brentano geometry using monochromatized Cu$K\alpha$ radiation (50 kV, 40 mA) and a step-scan technique in a 2θ range from 10° to 149.98° with a fixed counting time (t) of 15 s/step and a step interval ($\Delta 2\theta$) of 0.02°. Peak positions were determined after $K\alpha_2$ stripping on a computer program POWDERX [6], followed by the indexing procedure on a computer program TREOR90 [7]. In the latter procedure, 2θ values of 35 peak positions were used as input data. Only one monoclinic cell was found with satisfactory figures of merit $M_{20}/F_{20} = 35/42(0.007714, 62)$, $M_{30}/F_{30} = 27/34(0.007008, 0)$ and $M_{35}/F_{35} = 18/18(0.007997, 249)$ [8,9]. The derived unit-cell parameters, $a = 0.85592(11)$ nm, $b = 0.53086(7)$ nm, $c = 0.78954(10)$ nm and $\beta = 93.10(1)°$ were subsequently used as starting parameters in the next stage of the analysis.

Profile intensity data for refinement of unit-cell parameters were collected in a 2θ range from 10° to 80° with $t = 5$ s/step. Si powder was used as an internal standard reference material ($BaZr(PO_4)_2/Si = 2.33$ in weight). The unit-cell parameters were refined by the whole powder-pattern decomposition method, based on the Pawley algorithm [10], on a computer program WPPF [11]. The systematic peak shift $\Delta(2\theta)$ was corrected with the function $\Delta(2\theta) = t_0 + t_1 \cos 2\theta + t_2 \sin 2\theta$. During the decomposition process, the parameters $t_0 - t_2$ were refined together with the unit-cell parameters, while the unit-cell parameter of Si was fixed at a value of $a = 0.5430825$ nm [12]. The refined unit-cell parameters (Table 1) could index all reflections in the observed diffraction pattern. The refined integrated intensities were examined to confirm the presence and absence of reflections. There were systematic absences $h + k \neq 2n$ for $h\,k\,l$ reflections, implying that the possible space groups are $C2$, Cm, $C2/m$, Cc, and $C2/c$.

Table 1
Crystal data of barium zirconium diorthophosphate

Chemical composition	$BaZr(PO_4)_2$
Space group	$C2/m$
a (nm)	0.85629(3)
b (nm)	0.53082(2)
c (nm)	0.78956(2)
β (deg)	93.086(1)
V (nm^3)	0.35836(2)
Z	2
D_X (Mg m^{-3})	3.88

All of the possible space groups were tested using the EXPO package [13] for crystal structure determination. A minimum reliability index R_F [14] of 17.1% was obtained with the space group $C2/m$ in a default run of the program. Structural parameters of all atoms were refined by the Rietveld method on a computer program RIETAN-2000 [15] using the profile intensity data in the 2θ range of 19.0–149.98° (Fig. 1). The background intensities were fitted to a polynomial function with twelve adjustable parameters. The pseudo-Voigt function [16] was used to fit the peak profile. The systematic peak shift $\Delta(2\theta)$ was corrected with the function $\Delta(2\theta) = t_0 + t_1 \cos 2\theta + t_2 \sin 2\theta + t_3 \tan\theta$, while the unit-cell parameters were fixed throughout the refinement process. Isotropic atomic displacement parameters, B, were assigned to all atoms. Reliability indices for a final result were $R_{wp} = 8.21\%$, $R_p = 5.64\%$ and $R_B = 2.92\%$. [14]. Crystal data are given in Table 1, and final positional and displacement parameters of atoms are given in Table 2.

2.3. Thermal behavior

The thermal behavior was investigated up to 1473 K by a differential thermal analysis (DTA, Model TG8120, Rigaku Co., Tokyo, Japan). The temperature was controlled by a Pt–PtRh (10%) thermocouple, with heating and cooling rates of 10 K/min. The phase constitution as well as changes in cell parameters were examined by XRD equipped with a heating stage. The profile data with $t = 2$ s/step were collected in the 2θ range from 10° to 70° during stepwise heating up to 1173 K (step width = ~100 K). Powder specimens, mixed with Au powder as an internal temperature standard [17], were deposited with ethyl alcohol on the platinum heating filament (132 × 9 × 1 mm). A programmable divergence slit was employed to maintain an illumination length of 10 mm on the sample. Thus an

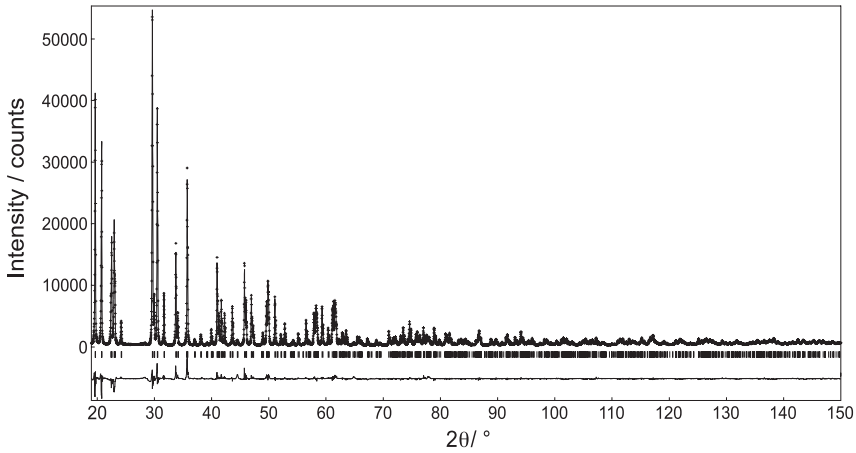

Fig. 1. Comparison between observed (+marks) and calculated (upper solid line) patterns of barium zirconium diorthophosphate. The difference curve is shown in the lower part of the figure. Vertical marks indicate the positions of possible Bragg reflections.

Table 2
Structural parameters of barium zirconium diorthophosphate

Atom	x	y	z	B (nm^2)
Ba	0	0	0.5	0.0064(3)
Zr	0	0	0	0.0010(4)
P	0.3624(2)	0	0.2223(2)	0.0031(5)
O1	0.2300(5)	0	0.0876(6)	0.009(1)
O2	0.3147(5)	0	0.4052(6)	0.007(1)
O3	0.4655(3)	0.2384(5)	0.1893(3)	0.002(1)

illumination area of 10×9 mm was realized regardless of the 2θ value. The cell parameters were refined by the WPPD method [11].

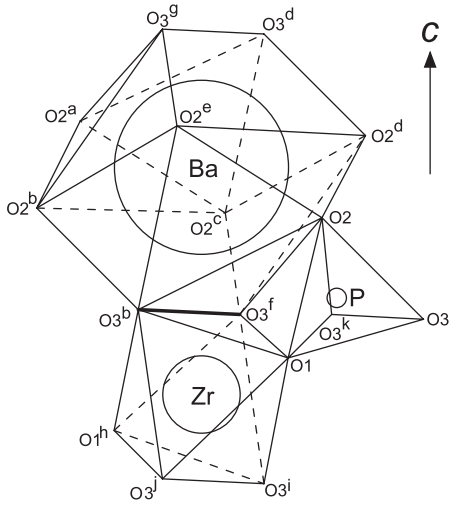

Fig. 2. Part of the structure viewed along [1$\bar{2}$0]. Atom numbering corresponds to that given in Table 2. Labels a, b, c, d, e, f, g, h, i, j and k correspond to the symmetry transformations in Table 3.

3. Results and discussion

3.1. Structure description

Fig. 2 shows a structure fragment of barium zirconium diorthophosphate. Selected interatomic distances and bond angles, together with their standard uncertainties, are listed in Table 3. Valence bond sums (Table 4) calculated on the basis of bond-strength analysis [18,19] are in good agreement with expected formal oxidation states of Ba^{2+}, Zr^{4+} and P^{5+} ions. Distortion parameters for the coordination polyhedra (Table 5) were determined using a computer program IVTON [20].

In the PO_4 tetrahedra the mean P–O bond length is 0.155 nm and the mean value of the O–P–O angles is 109°. These values are in good agreement with those found in other orthophosphates $Zr_2O(PO_4)_2$ [21], $CaZr(PO_4)_2$ [3] and $SrZr(PO_4)_2$ [1]. The Zr atom is sixfold coordinated with the mean Zr–O distance of 0.207 nm, which is comparable to those of the ZrO_6 octahedron in $CuZr_2(PO_4)_3$ (the mean = 0.207 nm) [22], $CaZr_4(PO_4)_6$ (0.206 nm) [23] and $K_2Zr(PO_4)_2$ (0.207 nm) [24]. The Ba atom is coordinated to ten oxygen atoms at distances ranging from 0.282 to 0.316 nm (the mean = 0.296 nm). A similar geometry around the Ba atom has been described in β-$BaV_2(P_2O_7)_2$ [25] and $BaTi_2(P_2O_7)_2$ [26]; the BaO_{10} polyhedron showed the bond lengths ranging from 0.276 to 0.311 nm (the mean = 0.292 nm) in the former structure and 0.281 to 0.307 nm (0.294 nm) in the latter.

Ionic radii of Ba^{2+} in the tenfold coordination [$r(Ba^{2+}(10)) = 0.152$ nm and $r(O^{2-}(8)) = 0.142$ nm] and Zr^{4+} in the sixfold coordination [$r(Zr^{4+}(6)) = 0.072$ nm and $r(O^{2-}(6)) = 0.140$ nm] predict the interatomic distances of 0.294 nm for Ba–O and 0.212 nm for Zr–O [27]. These predicted values are in good agreement with the corresponding mean interatomic distances of $\langle Ba-O \rangle = 0.296$ nm and $\langle Zr-O \rangle = 0.207$ nm.

Table 3
Coordinates of Ba, Zr and P

	O2	O2[a]	O2[b]	O2[c]	O2[d]	O2[e]	O3[b]	O3[f]	O3[d]	O3[g]
Ba										
O2	0.2835(7)	180.0(2)	114.2(2)	114.2(2)	65.8(2)	65.8(2)	80.0(1)	80.0(1)	100.0(1)	100.0(1)
O2[a]	0.5670(9)	0.2835(7)	65.8(2)	65.8(2)	114.2(2)	114.2(2)	100.0(1)	100.0(1)	80.0(1)	80.0(1)
O2[b]	0.5037(8)	0.3270(5)	0.3162(3)	114.2(2)	180.0(2)	65.8(2)	49.7(1)	100.3(1)	130.3(1)	79.7(1)
O2[c]	0.5037(8)	0.3270(5)	0.5308(0)	0.3162(3)	65.8(2)	180.0(2)	100.3(1)	49.7(1)	79.7(1)	130.3(1)
O2[d]	0.3270(5)	0.5037(8)	0.6323(5)	0.3436(9)	0.3162(3)	114.2(2)	130.3(1)	79.7(1)	49.7(1)	100.3(1)
O2[e]	0.3270(5)	0.5037(8)	0.3436(9)	0.6323(5)	0.5308(0)	0.3162(3)	79.7(1)	130.3(1)	100.3(1)	49.7(1)
O3[b]	0.3636(7)	0.4332(8)	0.2532(7)	0.4600(5)	0.5431(6)	0.3840(7)	0.2821(4)	59.0(2)	180.0(2)	121.0(2)
O3[f]	0.3636(7)	0.4332(8)	0.4600(5)	0.2532(7)	0.3840(7)	0.5431(6)	0.2778(6)	0.2821(4)	121.0(2)	180.0(2)
O3[d]	0.4332(8)	0.3636(7)	0.5431(6)	0.3840(7)	0.2532(7)	0.4600(5)	0.5642(6)	0.4910(6)	0.2821(4)	59.0(2)
O3[g]	0.4332(8)	0.3636(7)	0.3840(7)	0.5431(6)	0.4600(5)	0.2532(7)	0.4910(6)	0.5642(6)	0.2778(6)	0.2821(4)

	O1	O1[h]	O3[b]	O3[f]	O3[i]	O3[j]
Zr						
O1	0.2052(7)	180.0(3)	85.9(2)	85.9(2)	94.1(2)	94.1(2)
O1[h]	0.4103(9)	0.2052(7)	94.1(2)	94.1(2)	85.9(2)	85.9(2)
O3[b]	0.2810(7)	0.3019(7)	0.2073(4)	84.1(2)	180.0(2)	95.9(2)
O3[f]	0.2810(7)	0.3019(7)	0.2778(6)	0.2073(4)	95.9(2)	180.0(2)
O3[i]	0.3019(7)	0.2810(7)	0.4146(6)	0.3078(6)	0.2073(4)	84.1(2)
O3[j]	0.3019(7)	0.2810(7)	0.3078(6)	0.4146(6)	0.2778(6)	0.2073(4)

	O1	O2	O3	O3[k]
P				
O1	0.1512(7)	116.0(3)	106.9(3)	106.9(3)
O2	0.2572(9)	0.1522(7)	109.8(3)	109.8(3)
O3	0.2478(7)	0.2532(7)	0.1573(5)	107.1(3)
O3[k]	0.2478(7)	0.2532(7)	0.2530(6)	0.1573(5)

The values in diagonals are the central atom–ligand distances (nm), in the upper-right triangle the bond angles (deg) and in the lower left the ligand–ligand distances (nm) are given.
Symmetry transformations used to generate equivalent atoms: a: $-x, -y, 1-z$; b: $-1/2+x, -1/2+y, z$; c: $-1/2+x, 1/2+y, z$; d: $1/2-x, 1/2-y, 1-z$; e: $1/2-x, -1/2-y, 1-z$; f: $-1/2+x, 1/2-y, z$; g: $1/2-x, -1/2+y, 1-z$; h: $-x, -y, -z$; i: $1/2-x, 1/2-y, -z$; j: $1/2-x, -1/2+y, -z$; k: $x, -y, z$.

Table 4
Bond valence calculations

	Ba	Zr	P
O1		0.73	1.28
O1		0.73	
O2	0.23		1.25
O2	0.23		
O2	0.10		
O2	0.10		
O2	0.10		
O2	0.10		
O3	0.24	0.69	1.09
O3	0.24	0.69	1.09
O3	0.24	0.69	
O3	0.24	0.69	
V_i	1.8	4.2	4.7

$V_i = \Sigma_j \exp[(R_{ij} - d_{ij})/b]$ with $b = 0.037$ nm and $R_{ij} = 0.2285$ nm for Ba^{2+}, 0.1937 nm for Zr^{4+}, and 0.1604 nm for P^{5+}.

Table 5
Polyhedral distortion parameters

Polyhedron	Distortion parameters			
	Δ (nm)	r_s (nm)	σ	V_P (nm^3)
BaO_{10}	0.000	0.296	0.941	0.0499
ZrO_6	0.000	0.207	0.995	0.0116
PO_4	0.005	0.154	1	0.0019

Δ, eccentricity; r_s, radius of sphere fitted to ligands; σ, sphericity; V_P, volume of coordination polyhedron; σ for coordination number four is 1 by definition.

The crystal structure of barium zirconium diorthophosphate consists of the three types of polyhedra, BaO_{10}, PO_4 and ZrO_6. The former two polyhedra share edges to form two-dimensional sheets parallel to (001). These sheets are stacked in the [001] direction, and they are linked through the oxygen atoms O1 and O3 of the ZrO_6 octahedra to form a three-dimensional structure (Fig. 3). Since the atom arrangement is similar to that of yavapaiite ($KFe(SO_4)_2$), the crystal may be grouped into a large family of the yavapaiite-related compounds. However, the structures of $BaZr(PO_4)_2$ and $KFe(SO_4)_2$

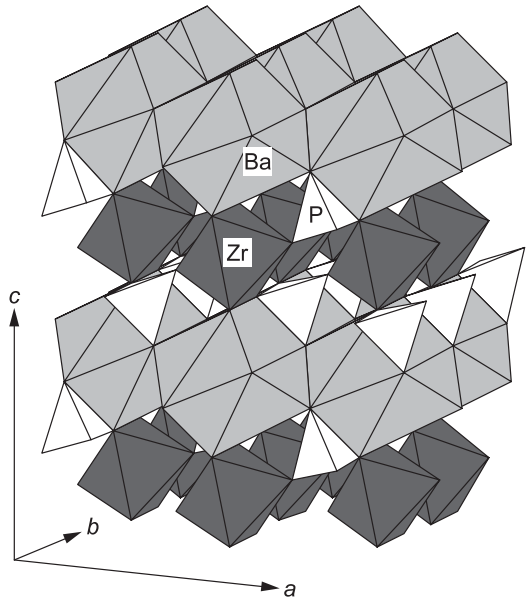

Fig. 3. Crystal structure of barium zirconium diorthophosphate.

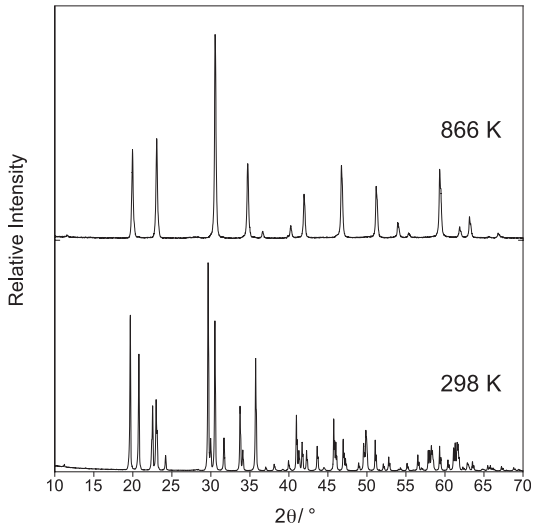

Fig. 4. Change in powder XRD pattern induced by the phase transition from monoclinic to orthorhombic during heating.

differ distinctly in the coordination numbers of barium and potassium atoms. One of the typical phosphates isostructural with yavapaiite would be $BaMo(PO_4)_2$; the barium atom is sixfold coordinated at distances ranging from 0.279 to 0.2795 nm (the mean = 0.279 nm) [28].

3.2. Phase transition during heating and cooling

The high-temperature XRD (Fig. 4) showed that, during the heating process up to 685 K, the crystal was exclusively composed of the monoclinic phase. For the profile intensity data taken at 866 K and above, all of the reflections were successfully indexed on an orthorhombic unit cell. The refined cell parameters at 866 K are $a = 0.9041(1)$ nm, $b = 0.5177(1)$ nm, $c = 0.7809(1)$ nm and $V = 0.3655(1)$ nm^3. The unit cell was nearly orthohexagonal ($\sqrt{3}b \approx a$), thus the reflections $2h0l$ and hhl closely overlapped. The integrated intensity parameters (I) and their estimated standard deviations [$\sigma(I)$] were also obtained by the WPPD method (Table 6). For the closely overlapping reflections, the individual intensities were equiportioned. Values of d-spacing (d_{calc}) and scattering angle ($2\theta_{calc}$) were determined from the unit-cell parameters. At 788 K during heating, the orthorhombic and monoclinic phases coexisted. The lattice correspondence between the two polymorphs are

$$\begin{bmatrix} \mathbf{a}_o \\ \mathbf{b}_o \\ \mathbf{c}_o \end{bmatrix} = \begin{bmatrix} 1 & 0 & 0 \\ 0 & 1 & 0 \\ 0 & 0 & 1 \end{bmatrix} \begin{bmatrix} \mathbf{a}_m \\ \mathbf{b}_m \\ \mathbf{c}_m \end{bmatrix},$$

where $\mathbf{a}_m$, $\mathbf{b}_m$ and $\mathbf{c}_m$ are the lattice vectors of the monoclinic phase, $\mathbf{a}_o$, $\mathbf{b}_o$ and $\mathbf{c}_o$ are those of the orthorhombic phase.

The endothermic effect of DTA at 732 K during heating was assigned as the phase transition from monoclinic to orthorhombic. The exothermic effect of DTA at 710 K during cooling would be due to the reverse phase transition. The changes in cell dimensions with increasing temperature, together with the transition temperature, are shown in Fig. 5. The monoclinic-to-orthorhombic phase transition during heating was accompanied by a slight increase in unit-cell volume by 0.5%; the a_m-axis expanded by 4.2%, and the b_m- and c_m-axes shrank by 2.3% and 1.4%, respectively.

3.3. Anisotropic thermal expansion

With increasing temperature from 298 to 685 K, the a_m- and c_m-axes of the monoclinic phase increased and the β-angle decreased (Fig. 5). The b_m-axis showed a very slight contraction during heating. The unit-cell volume as a result steadily increased and the volumetric expansion due to an increment in temperature from 298 to 685 K was 1.5%.

The initial crystal lattice at 298 K will be, when heated at higher temperatures, homogeneously distorted into the new crystal lattice. Because of the monoclinic symmetry for the crystal up to 732 K, one of the principal axes of distortion is parallel to the b_m-axis; however, the others do not coincide with the a_m- or with the c_m-axes. The directions and magnitudes of the principal distortions upon heating from 298 K to T are, respectively, given by the eigenvectors and eigenvalues (λ_i) of the following equation [29–34]:

$$|G_T - G_{298\,K}\lambda_i^2| = 0, \quad (1)$$

Table 6
Powder XRD data of the orthorhombic phase at 866 K[a]

h	k	l	d_{calc} (nm)	$2\theta_{calc}$ (deg)	I	$s(I)$	I_{calc}
0	0	1	0.7809	11.32	23.2	3.2	2
2	0	0	0.4520	19.62	597.7	6.5	39
1	1	0	0.4493	19.74	597.7		39
2	0	1	0.3912	22.71	491.9	4.8	32
0	0	2	0.3904	22.76	491.9		32
1	1	1	0.3894	22.82	491.9		32
2	0	2	0.2955	30.22	1535.3	10.1	100
1	1	2	0.2947	30.30	1535.3		100
3	1	0	0.2604	34.41	404.3	4.4	26
0	0	3	0.2603	34.43	404.3		26
0	2	0	0.2589	34.62	404.3		26
3	1	1	0.2471	36.33	80.2	13.2	5
0	2	1	0.2457	36.54	23.0	13.0	1
4	0	0	0.2260	39.85	49.2	1.5	3
2	0	3	0.2256	39.94	49.2		3
1	1	3	0.2252	40.00	49.2		3
2	2	0	0.2246	40.11	49.2		3
4	0	1	0.2171	41.56	175.3	2.6	11
3	1	2	0.2167	41.65	175.3		11
2	2	1	0.2159	41.81	175.3		11
0	2	2	0.2158	41.83	175.3		11
4	0	2	0.1956	46.38	413.4	4.5	27
0	0	4	0.1952	46.48	413.4		27
2	2	2	0.1947	46.61	413.4		27
3	1	3	0.1841	49.47	6.4	1.8	<1
0	2	3	0.1835	49.63	6.4		<1
2	0	4	0.1792	50.91	451.0	5.8	29
1	1	4	0.1790	50.96	451.0		29
5	1	0	0.1707	53.65	51.2	1.4	3
4	0	3	0.1707	53.66	51.2		3
4	2	0	0.1703	53.80	51.2		3
2	2	3	0.1701	53.86	51.2		3
1	3	0	0.1695	54.05	51.2		3
5	1	1	0.1668	55.02	35.8	4.8	2
4	2	1	0.1663	55.17	35.8		2
1	3	1	0.1657	55.42	2.1	9.1	<1
5	1	2	0.1564	59.01	205.2	2.3	13
3	1	4	0.1562	59.09	205.2		13
0	0	5	0.1562	59.11	205.2		13
4	2	2	0.1561	59.15	205.2		13
0	2	4	0.1559	59.23	205.2		13
1	3	2	0.1555	59.39	205.2		13

[a]Cell dimensions: a=0.9041(1) nm, b=0.5177(1) nm, c=0.7809(1) nm and V = 0.3655(1) nm^3.

where $\mathbf{G}_{298\,K}$ is the metric for the initial lattice at 298 K and $\mathbf{G}_T$ is the metric for the product lattice at T. The metric for the monoclinic phase is given by

$$\mathbf{G}_T = \begin{bmatrix} a_T^2 & 0 & a_T c_T \cos\beta_T \\ 0 & b_T^2 & 0 \\ a_T c_T \cos\beta_T & 0 & c_T^2 \end{bmatrix},$$

where a_T, b_T, c_T and β_T are the cell dimensions at T. In the orthonormal basis defined by the principal axes of distortion, the matrix ($\mathbf{D}_T$), which represents the lattice deformation, takes the simple form

$$\mathbf{D}_T = \begin{bmatrix} \lambda_1 & 0 & 0 \\ 0 & \lambda_2 & 0 \\ 0 & 0 & \lambda_3 \end{bmatrix}.$$

Eq. (1) was solved to determine the directions and magnitudes of the three principal distortions. With increasing temperature to 685 K, both magnitudes of λ_1 and λ_3 showed a steady increase to 1.0153(2) and 1.0013(1), respectively (Fig. 6). The magnitude of λ_1 was the largest at any temperature and about 15 times that of λ_3 at 685 K. On the other hand, λ_2 showed a tendency to steadily decrease to 0.9987(1). The mean principal distortion λ_m, which is determined by $[\lambda_1+\lambda_2+\lambda_3]/3$, steadily increased to 1.0051(1) with increasing temperature to 685 K. The mean linear thermal expansion coefficient (α_m) was derived from the mean principal strain ($\lambda_m - 1$) as follows:

$$a_m = (\lambda_m - 1)/\Delta T[K^{-1}].$$

The coefficient over the temperature range from 298 to 685 K was $1.32(4)\times10^{-5}\,K^{-1}$.

The directions of the three principal distortions are, for example, at T = 685 K, expressed as

$$\boldsymbol{\lambda_1} = 0.932(1)\mathbf{i} + 0.363(3)\mathbf{k},$$
$$\boldsymbol{\lambda_2} = \mathbf{j},$$
$$\boldsymbol{\lambda_3} = -0.363(3)\mathbf{i} + 0.932(1)\mathbf{k},$$

where **i**, **j** and **k** are the unit vectors in the orthonormal basis defined by $\mathbf{i}//a^*$, $\mathbf{j}//b$ and $\mathbf{k}//c$. The directions of $\boldsymbol{\lambda_1}$ and $\boldsymbol{\lambda_3}$ are, respectively, nearly parallel to [201] and [$\bar{1}$03]; the intersection angles are 1.2° ($=\lambda_1$ ^ [201]) and 1.5° ($=\lambda_3$ ^ [$\bar{1}$03]). The directions of λ_1 and λ_3 were simply represented by the angle λ_1 ^ c (Fig. 7). During heating from 394 to 685 K, the angle steadily increased from 63.3(9)° to 68.7(2)°. At 394 K, the directions of λ_1 and λ_3 are, respectively, nearly parallel to [503] and [$\bar{1}$02] (λ_1 ^ [503] = 0.1° and λ_3 ^ [$\bar{1}$02] = 1.1°).

For the orthorhombic phase, where the principal distortion axes exactly coincide with the crystallographic axes, the magnitude of λ_3 ($=c_T/c_{866\,K}$) showed a steady increase to 1.0095(3) with increasing temperature from 866 to 1173 K (Fig. 5(c)). On the other hand, the λ_1 ($=a_T/a_{866\,K}$) and λ_2 ($=b_T/b_{866\,K}$) showed relatively small thermal change during the heating process (Figs. 5(a) and (b)). Thus, the crystal as a whole showed the thermal expansion of about 1.0% in volume and 0.3% in mean principal distortion λ_m. The mean linear expansion coefficient from 866 to 1173 K was $9.6(6)\times10^{-6}\,K^{-1}$.

The crystal structures at ambient temperature and polymorphic sequences are now revealed for the double phosphates $MZr(PO_4)_2$ (M = Ca, Sr and Ba). The structure of $CaZr(PO_4)_2$ is rather distinct from those of the others. The monoclinic phase of $SrZr(PO_4)_2$,

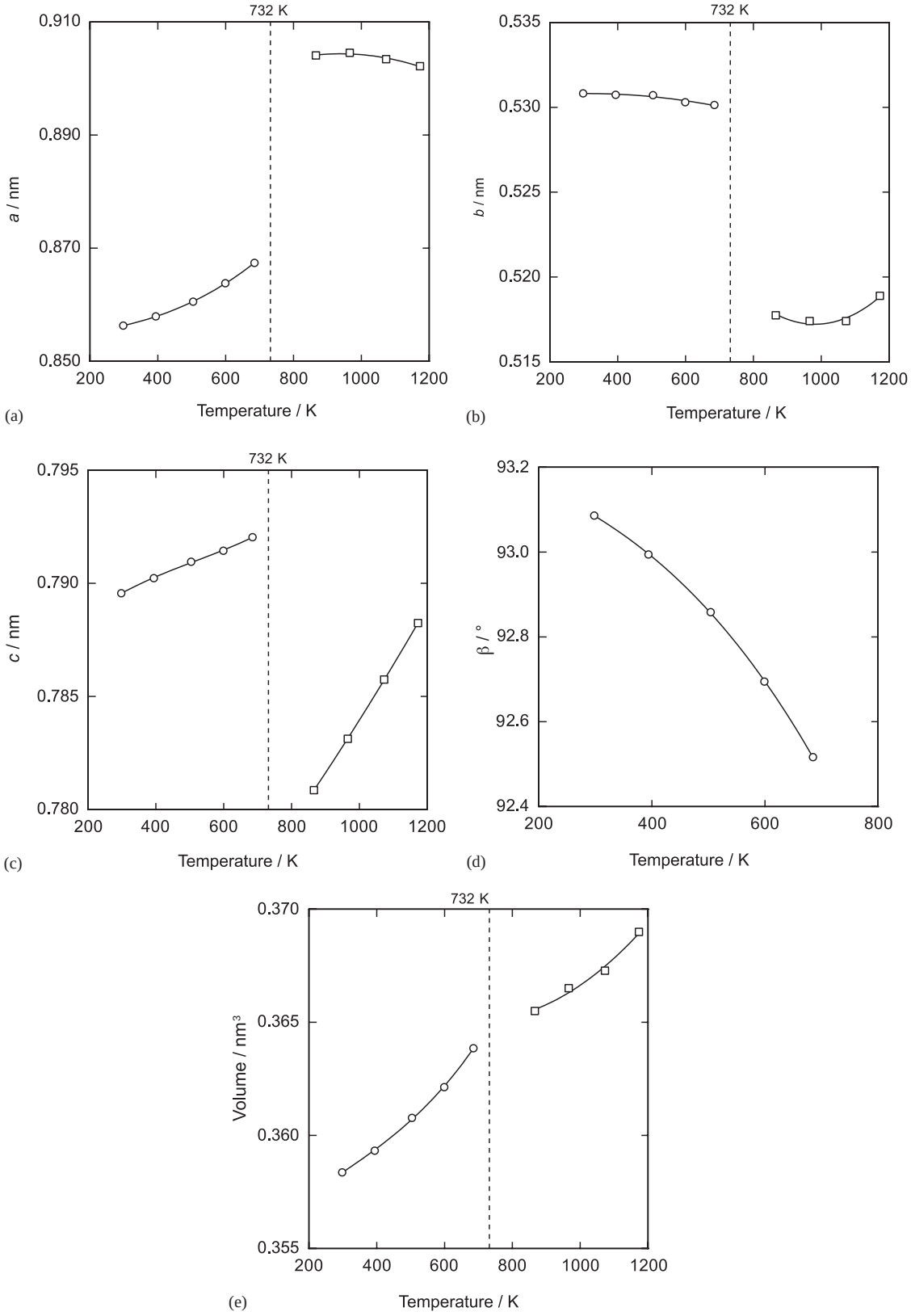

Fig. 5. Variation of cell parameters with temperature. (a) a, (b) b, (c) c, (d) β and (e) volume. The polymorphic phase transition from monoclinic to orthorhombic occurs at 732 K during heating.

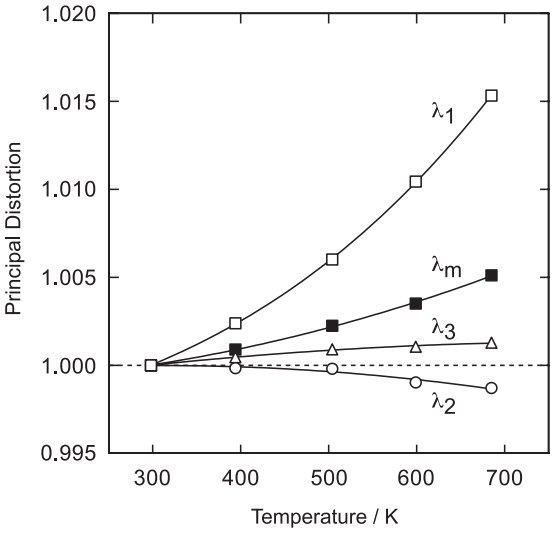

Fig. 6. Temperature dependence of principal distortions (λ_i, $i = 1$, 2 and 3) for the monoclinic phase from 298 to 685 K. The mean principal distortion λ_m is determined by $[\lambda_1 + \lambda_2 + \lambda_3]/3$.

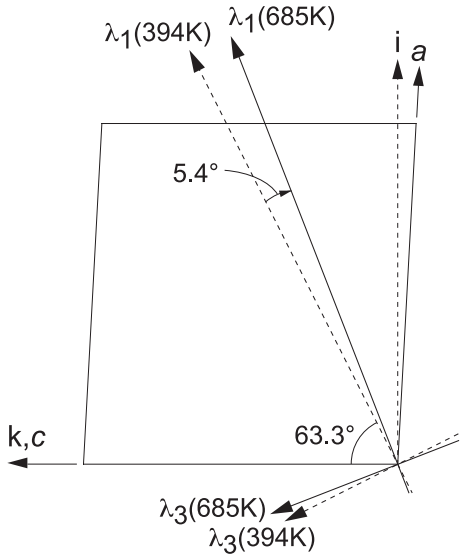

Fig. 7. Superposition of the principal axes λ_1 and λ_3 on the monoclinic unit cell at 298 K. The angle λ_1 ^c is used to define the orientation of the principal axes. The λ_2-axis coincide with the crystallographic b-axis.

being stable at high temperatures, is most probably isostructural with the monoclinic $BaZr(PO_4)_2$. Because the atom arrangement of the latter is similar to that of yavapaiite, the $SrZr(PO_4)_2$ and $BaZr(PO_4)_2$ crystals may be grouped into a large family of the yavapaiite-related compounds.

4. Conclusion

We determined the crystal structure of $BaZr(PO_4)_2$ at 298 K, being monoclinic with space group $C2/m$. The Ba atom is tenfold coordinated with a mean Ba–O distance of 0.296 nm. The Zr atom is coordinated to six oxygen atoms at a mean distance of 0.207 nm. The BaO_{10} and PO_4 polyhedra share edges to form two-dimensional sheets parallel to (001). These sheets are stacked in the [001] direction, and they are connected through ZrO_6 octahedra to form a three-dimensional structure. During heating, the monoclinic-to-orthorhombic phase transition occurred at 732 K. Both phases showed relatively strong anisotropy in thermal expansion.

References

[1] K. Fukuda, A. Moriyama, S. Hashimoto, J. Solid State Chem. 177 (2004) 3514–3521.
[2] E.J. Graeber, A. Rosenzweig, Am. Mineral. 56 (1971) 1917–1933.
[3] K. Fukuda, K. Fukutani, Powder Diffr. 18 (2003) 296–300.
[4] G.S. Zhdanov, in: A.F. Brown (Ed.), Crystal Physics, Oliver & Boyd Press, Edinburgh, UK, 1965, pp. 411–420.
[5] J.F. Nye, Physical Properties of Crystals, The Clarendon Press, Oxford, UK, 1957, pp. 63–109.
[6] C. Dong, J. Appl. Crystallogr. 32 (1999) 838.
[7] P.E. Werner, L. Eriksson, M. Westdahl, J. Appl. Crystallogr. 18 (1985) 367–370.
[8] P.M. de Wolff, J. Appl. Crystallogr. 1 (1968) 108–113.
[9] G.S. Smith, R.L. Snyder, J. Appl. Crystallogr. 12 (1979) 60–65.
[10] G.S. Pawley, J. Appl. Crystallogr. 14 (1981) 357–361.
[11] H. Toraya, J. Appl. Crystallogr. 19 (1986) 440–447.
[12] C.R. Hubbard, J. Appl. Crystallogr. 16 (1983) 285–288.
[13] A. Altomare, M.C. Burla, M. Camalli, B. Carrozzini, G.L. Cascarano, C. Giacovazzo, A. Guagliardi, A.G.G. Moliterni, G. Polidori, R. Rizzi, J. Appl. Crystallogr. 32 (1999) 339–340.
[14] R.A. Young, in: R.A. Young (Ed.), The Rietveld Method, Oxford University Press, Oxford, UK, 1993, pp. 1–38.
[15] F. Izumi, T. Ikeda, Mater. Sci. Forum 198 (2000) 321–324.
[16] H. Toraya, J. Appl. Crystallogr. 23 (1990) 485–491.
[17] R.O. Simmons, J. Appl. Phys. 41 (1970) 2235–2240.
[18] I.D. Brown, D. Altermatt, Acta Crystallogr. B 41 (1985) 244–247.
[19] N.E. Brese, M. O'Keeffe, Acta Crystallogr. B 47 (1991) 192–197.
[20] T. Balic-Zunic, I. Vickovic, Acta Crystallogr 29 (1996) 305–306.
[21] W. Gebert, E. Tillmanns, Acta Crystallogr. B 31 (1975) 1768–1770.
[22] I. Bussereau, M.S. Belkhiria, P. Gravereau, A. Boireau, J.L. Soubeyroux, R. Olazcuaga, G. Le Flem, Acta Crystallogr. C 48 (1992) 1741–1744.
[23] J. Alamo, J.L. Rodrigo, J. Solid State Chem. 63–65 (1993) 678–683.
[24] M. Dorffel, J. Liebertz, Z. Kristallogr. 193 (1990) 155–159.
[25] S.-J. Hwu, R.I. Carroll, D.L. Serra, J. Solid State Chem. 110 (1994) 290–294.
[26] S. Wang, S.-J. Hwu, J. Solid State Chem. 90 (1991) 31–41.
[27] R.D. Shannon, Acta Crystallogr. A 32 (1976) 751–767.
[28] A. Leclaire, M.M. Borel, J. Chardon, B. Raveau, J. Solid State Chem. 116 (1995) 364–368.
[29] J.W. Christian, The Theory of Transformations in Metals and Alloys, Pergamon Press, Oxford, UK, 1975, pp. 40–48.
[30] K. Fukuda, I. Maki, S. Ito, J. Am. Ceram. Soc. 80 (1997) 1595–1598.
[31] K. Fukuda, J. Ceram. Soc. Jpn. 109 (2001) 830–850.
[32] K. Fukuda, K. Yamauchi, J. Mater. Res. 17 (2002) 1050–1054.
[33] K. Fukuda, H. Matsubara, J. Mater. Res. 18 (2002) 1715–1722.
[34] K. Fukuda, H. Matsubara, J. Am. Ceram. Soc. 87 (2004) 89–92.